CHAPTER 4

Positron Emission Imaging in Chemical Engineering

J.P.K. Seville[1,*], A. Ingram[2], X. Fan[3] and **D.J. Parker[3]**

Contents

Abstract

Better understanding, design and operation of engineering processes demand visualisation of the material flows within them under realistic conditions. Methods based on radioactive tracers

1 School of Engineering, University of Warwick, Coventry CV4 7AL, UK

2 School of Chemical Engineering, University of Birmingham, Birmingham B15 2TT, UK

3 School of Physics and Astronomy, University of Birmingham, Birmingham B15 2TT, UK

*Corresponding author.
E-mail address: J.P.K.Seville@warwick.ac.uk

Advances in Chemical Engineering, Volume 37
ISSN: 0065-2377, DOI 10.1016/S0065-2377(09)03704-1

enable visualisation to be performed on real processes taking place within opaque walls. Positron emission methods rely on detecting the pairs of back-to-back gamma rays produced when a positron (emitted in radioactive decay) annihilates with an electron, and are variants of positron emission tomography (PET) which is widely used in medicine for determining the distribution in 3D of a labelled fluid. In chemical engineering applications, extensive use has been made of the alternative technique of positron emission particle tracking (PEPT), invented at the University of Birmingham, in which a single tracer particle is radioactively labelled and can be accurately tracked at high speed. This has now been developed to the point where it has the capability to track tracer particles down to approximately 60 μm in size, moving at up to 10 m/s, yielding locations to within ±1 mm at frequencies better than 100 Hz. Most importantly, gamma rays are sufficiently penetrating that good location data can be obtained within real process vessels. Applications have been extremely diverse, and include both gas-phase-continuous and liquid-phase-continuous systems. Particularly strong contributions have been made to the study of mixing processes and applications of fluidisation. Hitherto, the method has been confined to the laboratory. However, a modular transportable positron camera has now been developed and has been used for the first time on large-scale plant at an industrial site.

1. INTRODUCTION

Better understanding, design and operation of engineering processes demand visualisation of the material flows within them under realistic conditions. The range of techniques available for imaging industrial processes is vast (Chaouki et al., 1997). A fundamental distinction can be made between (a) projection-imaging techniques, exemplified most simply by conventional photography, (b) tomographic techniques, in which an image is obtained of a slice through an object, and (c) particle tracking techniques, such as those which employ a radioactive tracer. The interest here is in techniques that can be used to image processes taking place within metal-walled vessels. This rules out most of the optical and electrical methods and places the emphasis on x-ray and radioactive techniques.

Within the radiation emission tracking techniques, there are two main variants: positron emission, in which the tracer position is determined by triangulation as described in Section 2, and the "proximity" techniques, in which a gamma emitter is placed within the system of interest and its position found by measuring the relative count rates in an array of detectors. An example of the latter is computer-automated radioactive

particle tracking technique (CARPT) developed at the University of Washington St. Louis and the École Polytechnique, Montréal. Both can be used to image material flows in industrial processes and both have advantages and disadvantages. One major difference between them, however, is that proximity techniques require extensive experimental calibration and pre-calculation to take account of the effect of the vessel walls, whereas positron emission methods do not require this. In both cases, a feature of particular benefit to engineering studies is the fact that the actual particles of interest may be used as tracers, rather than dissimilar materials of unknown behaviour.

2. POSITRON EMISSION TECHNIQUES AND THEIR RECENT DEVELOPMENT

2.1 Positron emission particle tracking (PEPT) and positron emission tomography (PET)

Positron emission particle tracking (PEPT) is derived from the commonly used medical diagnostic technique of positron emission tomography (PET). The main difference is that in PET a distribution of radioactivity is imaged in a relatively long time (some minutes), whereas in PEPT a single small source of radioactivity is located very frequently (normally up to approximately 100 times per second). The basis of all positron-imaging methods is that positrons emitted from the tracer annihilate with free electrons very close to their point of emission to produce pairs of ''back-to-back'' γ-rays, which travel along the same line in opposite directions. These are then detected using two large position-sensitive detectors (the ''positron camera''), from which, in PEPT, a line can be constructed on which the tracer particle must lie (as shown in Figure 1). In theory, two such lines are sufficient to locate the tracer in three dimensions; in practice, normally approximately 100 are used. An algorithm

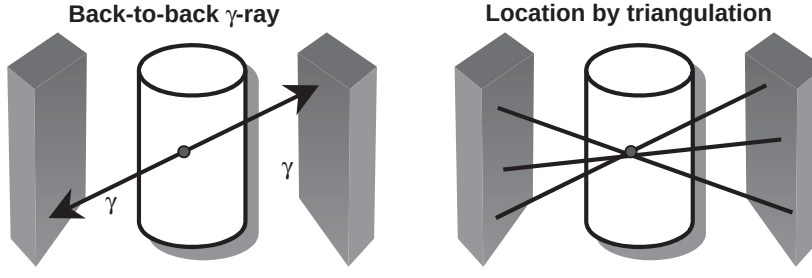

Figure 1 Principles of PEPT.

then finds the most probable position of the tracer by eliminating the outliers from the set of γ lines.

A significant number of the detected events are invalid, as either they correspond to a "random coincidence" between two unrelated γ-rays or else one or both of the γ-rays has been scattered before detection. The PEPT algorithm attempts to discard these invalid events, using an iterative procedure in which the centroid of the events is calculated, the γ-rays passing furthest from the centroid are discarded, and this process is repeated until a specified fraction f of the original events remains. The optimum value of f depends on the mass of material between the tracer and the detectors, which adds to the number of scattered events. For example, when studying flow inside a vessel with 15 mm thick steel walls, 80% of the detected events must be discarded, so that the fraction f of useful events is 0.2. The precision Δ of a PEPT location is given approximately by

$$\Delta \approx \frac{w}{\sqrt{fN}} \tag{1}$$

where w is the intrinsic spatial resolution of the positron camera (roughly 10 mm in a conventional camera), N the number of events detected during the location interval and f the fraction of these actually used for location. Assuming a data rate of $50\,\mathrm{k\,s^{-1}}$ with $f = 0.2$ one expects to be able to locate the tracer to within approximately 1 mm every 10 ms using the existing camera. This is typical of the tracking achieved for relatively slow moving tracers. During this time interval a tracer moving at 1 m/s will move 10 mm, so that for faster moving tracers it is necessary to locate more frequently and with slightly lower precision.

Features of PEPT of particular benefit to engineering studies include the fact that the actual particles of interest may be used as tracers, rather than dissimilar materials of unknown behaviour, and that γ-rays are sufficiently penetrating that location is unimpaired by the presence of metal walls, for example. In recent developments, the minimum size of particles which can be tracked has been reduced to approximately 60 μm. It is now possible to track multiple particles, to determine particle rotation and to track motion within real industrial equipment by use of a mobile modular positron camera. These developments are described later.

Figure 2 shows examples of how the data from PEPT can be treated, in this case from a spouted bed. The simplest data output is a continuous trajectory, consisting of a large file of x, y, z, time values, plus optional continuously recorded user-defined parameters such as speed or blade position. Velocity values can be obtained from this data file, in practice by a multi-point weighted averaging technique, and time averaged velocity profiles can then be derived. It is also possible to obtain values of

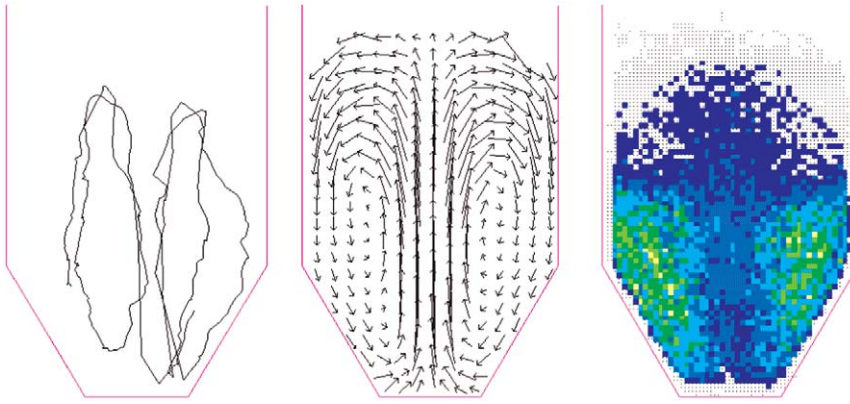

Figure 2 Typical PEPT output for a spouted bed (Left to Right: single trajectory; time-averaged velocity vectors; time-averaged "occupancy", showing denser annular region and leaner spout region) (see Plate 8 in Color Plate Section at the end of this book).

"occupancy", the proportion of the total run time which the tracer particle spends in each volume element of the object under scrutiny, which is equivalent to time averaged density. All time averaging — of velocities and occupancies — relies on the principle of "ergodicity", that is, that following one particle for a long time is equivalent to following all particles for a short time. Obviously this condition is not always satisfied, particularly when the process in question is time varying, but for many processes in laboratory-scale equipment this condition is satisfied for run times of order 1 h. As the scale increases, so must the run time.

More complex measures of particle behaviour can be obtained by further analysis of PEPT data, as described later.

2.2 Positron-emitting tracers

In most PEPT studies, it is desirable that the tracer particle should have properties indistinguishable from the bulk material. A major emphasis in PEPT-related research has been extending the range of tracer particles available to users, by developing a set of labelling techniques which are appropriate to a wide range of applications (Fan et al., 2006a, b, c). The original approach of direct irradiation in the ^{3}He beam from a cyclotron to generate ^{18}F (half-life 110 min) from oxygen *in situ* was limited to larger particles of high melting point oxides. Using alternative techniques of attaching ^{18}F from solution (produced when pure water is irradiated in the cyclotron beam), a wide range of tracers can now be made. As a result, the minimum tracer size has been reduced in stages from 600 μm to 60 μm for a variety of candidate materials. In most cases,

this requires surface chemistry development tailored to the application, introducing bridging ions such as Fe^{3+}.

^{18}F is convenient to produce and process, but has the disadvantage that when tracers are exposed to aqueous environments the attached fluoride rapidly leaches back into solution. For early PEPT studies in water this problem was crudely overcome by painting the surface of the tracer particle with cellulose paint to seal in the activity, but inevitably this can alter the behaviour of the tracer. Recently, techniques have been developed for labelling small particles with ^{61}Cu (half-life 3.4 h) and ^{66}Ga (9.3 h), which survive much better in an aqueous environment. These radioisotopes are produced by irradiating metal foils (^{61}Cu from natural Ni in the reaction $^{60}Ni(d,n)^{61}Cu$ and ^{66}Ga from natural Zn in the reaction $^{66}Zn(p,n)^{66}Ga$) and are then chemically separated using a cation-exchange process, which is significantly more selective than the standard anion-exchange process. In the future, it may become practical to produce and separate ^{64}Cu (12.7 h). The longer-lived nuclides like ^{66}Ga and ^{64}Cu have obvious advantages if PEPT is to be used *in situ*, as discussed in Section 4.

Tracers labelled with ^{61}Cu and ^{66}Ga are suitable for use in aqueous environments, but like most indirectly labelled particles lose their activity rapidly in abrasive systems. For such environments, and also for high temperature applications, directly activated particles are currently preferred, since the radioactivity is incorporated in the matrix rather than attached to the surface. The Positron Imaging Centre at Birmingham has continued to develop direct activation of high melting point oxides (silica, alumina, etc.) and also of small copper particles (producing ^{64}Cu *in situ* through the reaction $^{63}Cu(d,p) \rightarrow {}^{64}Cu$). It is difficult to activate very small particles in this way, partly because of practical issues in mounting the particles and focussing the cyclotron beam onto them, but more fundamentally because the heating effect of a highly focussed beam destroys the particles unless they are extremely well cooled.

2.3 Detectors

The original Birmingham positron camera consisted of a pair of rectangular gas-filled multi-wire chambers with rather low sensitivity for detecting the 511 keV γ-rays from positron annihilation. Its successor, an ADAC Forte, has similar geometry (two NaI(Tl) gamma camera heads, each $50 \times 40\,cm^2$) but significantly higher sensitivity and count rate capability. Under optimum conditions this camera records up to 100k coincidence events per second, enabling a tracer to be located to within 1 mm once per millisecond. The characteristics of this camera have been fully described by Parker et al. (2002).

Scanners used for medical PET generally adopt an entirely different approach, using rings of many individual small γ-ray detectors, giving even greater sensitivity and count rate. The geometry of a standard medical scanner is unsuited for many engineering studies (this is one reason why few engineering PET studies have been reported using hospital scanners), but since the architecture of these scanners is inherently modular it is in principle possible to reconfigure them into alternative geometries. This has been done using a donated ex-hospital PET scanner, which has been completely rebuilt as a modular positron camera for performing PEPT studies over a range of length scales: it is transportable and has been used for a series of PEPT studies on a large scale fluidised bed on an industrial site, as described in Section 4. When configured in a compact geometry it achieves a count rate of over 300k events per second, allowing very accurate high-speed tracking, and has been used in this way to study granular motion in high-speed rotating equipment.

2.4 Technique development

Although PEPT is extremely powerful, there are limits to the information that can be obtained by tracking a single particle. In a well-mixed steady-state system, the single particle, if followed for long enough, can demonstrate all features of the flow. However, to observe transients or particle–particle correlations requires simultaneous tracking of more than one particle. The original PEPT algorithm relies on *a priori* knowledge that only a single labelled particle is present in the field of view, and proceeds iteratively to discard outlying events until only a tight cluster of events remains. This algorithm has recently been extended to enable several particles to be tracked simultaneously, the first time that this has been done (Yang et al., 2006, 2007a, b). The standard PEPT algorithm is used to locate one of the tracers (discarding events corresponding to all other tracers), then the discarded data is re-examined and used to find a second tracer, and so on. This approach works reasonably well provided the tracers do not approach very close to each other. The particles can be distinguished if their activities are significantly different.

Multi-particle tracking is obviously of use in studies of segregation, where particles are separated in processing by virtue of differences in their size or density or both. These include fluidisation and gravity-driven flows. A special case of the technique is where three tracers are attached to different points on a larger body — multi-particle tracking can then be used to follow the rotational as well as translational motion of this body. This approach has been applied, for example, to observe the motion of lumps of foodstuff inside rotating cans during heat sterilisation.

3. APPLICATIONS

Applications of positron imaging, particularly PEPT, have been extensive and very diverse. In general, they vary from quick diagnostic studies for industrial users to fundamental work on multi-phase systems, such as ''granular gases'' (see, e.g., Wildman et al., 2005). Here, we concentrate on work aimed at industrial understanding.

3.1 Fluidised beds

PEPT has been used extensively in fluidised beds. Applications have included: solids circulation and measurement of the characteristic ''turnover time'' (Stein et al., 2000); scaling studies for solids motion (Stein et al., 2002); motion around in-bed obstacles such as heat-exchange surfaces (Ding et al., 2001b); the effect of cohesion in fluidisation due to surface liquid layers (Seville et al., 2000) and to sintering at high temperature (Seville et al., 1998, 2004); heat transfer by particle convection to in-bed tubes (Wong and Seville, 2006); segregation (Leaper et al., 2004); solids motion in circulating fluidised beds (CFB) (van de Velden et al., 2008); coating in top-spray fluidised beds (Depypere et al., 2009), bottom-spray Wurster coaters (Palmer et al., 2007; Palmer, 2008) and spouted beds (Seiler et al., 2008); and validation of computational approaches to the modelling of fluidised beds (Hoomans et al., 2001; Link et al., 2008).

From a practical point of view, one of the most challenging applications to date has been in the experimental fluidised bed shown in Figure 3, which is a scaled-down version of a polyethylene production unit, of overall height approximately 2 m, with a conical expansion section 1 m above the distributor; the diameter of the lower section is 0.154 m. The bed is constructed of 316 stainless steel and is placed within a gas circulation loop allowing operation at pressures up to 20 bars.

3.1.1 Solids motion studies

Figure 4 shows a typical projection of a (3D) particle trajectory. The essential features of all such trajectories, which we have investigated in previous publications (Stein et al., 2000), are as follows:

- Particles move upwards in a series of discrete fast movements (''jumps''), punctuated by periods of relative inactivity (''idle time'' or ''quiescent time''). It is during these idle times that the particles are able to sinter in polymer reactors, and control of the length of these periods is necessary to prevent defluidisation by sintering (Seville et al., 1998).
- Jumps are associated with bubble motion.

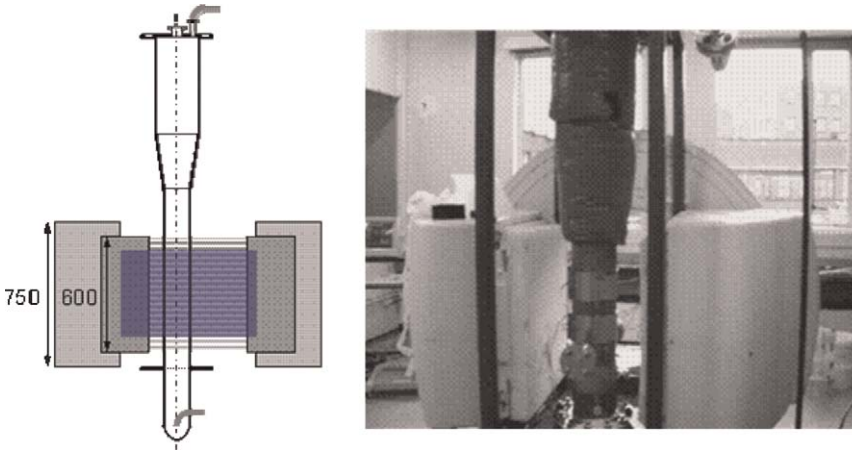

Figure 3 Pressurised fluidised bed-imaging geometry: schematic (left; dimensions in mm), and photograph (right).

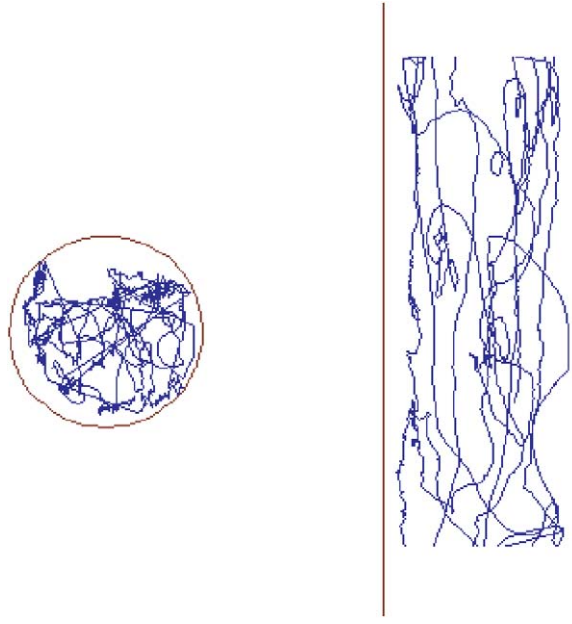

Figure 4 Typical fluidised bed trajectories (Left: plan; Right: elevation).

- Although the average jump velocity and average distance jumped increase with increasing gas velocity, the jump duration stays relatively constant; a theoretical explanation for this is given by Stein et al. (2000).
- Particles move down relatively slowly and (usually) near to the wall.
- The lengths of the trajectories form a wide distribution — not all upward movements terminate with ejection into the freeboard and not all downward movements terminate at the distributor.

Having obtained a trajectory as in Figure 4, it is possible to apply two virtual surfaces within the bed, for example, at heights of one quarter and three quarters of the settled bed height, and to record the times of crossing these surfaces. This enables cycle durations and frequencies to be obtained, which can be useful in diagnosing performance issues.

3.1.2 Motion close to surfaces

Fluidised beds are particularly favoured as chemical reactors, because of their ability to exchange heat through immersed heat exchange surfaces. However, little is known about how the heat exchange process works on a single particle level. The most commonly applied theory of fluidised bed heat exchange is that developed by Mickley and Fairbanks (1955) — the so-called ''packet model''. Wong and Seville (2006) used PEPT to follow the trajectory of a single tracer particle in a fluidised bed containing heat exchanger tubes. The residence time of particles in the vicinity of the heat exchange surface was determined directly for the first time, allowing the observed heat transfer variations to be interpreted mechanistically

Locational inaccuracy means that it is not possible to determine with certainty whether the tracer makes contact with the tube surface. Therefore, the method shown schematically in Figure 5 was adopted: a notional cylindrical surface is drawn around the heat transfer tube at a certain distance from it, and the time for which the tracer remains within this outer surface is determined. This is termed the residence time.

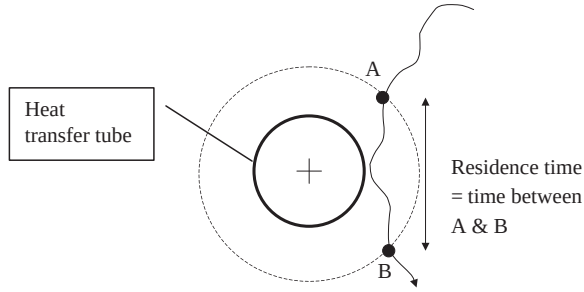

Figure 5 Residence time determination using particle trajectory (Wong and Seville, 2006).

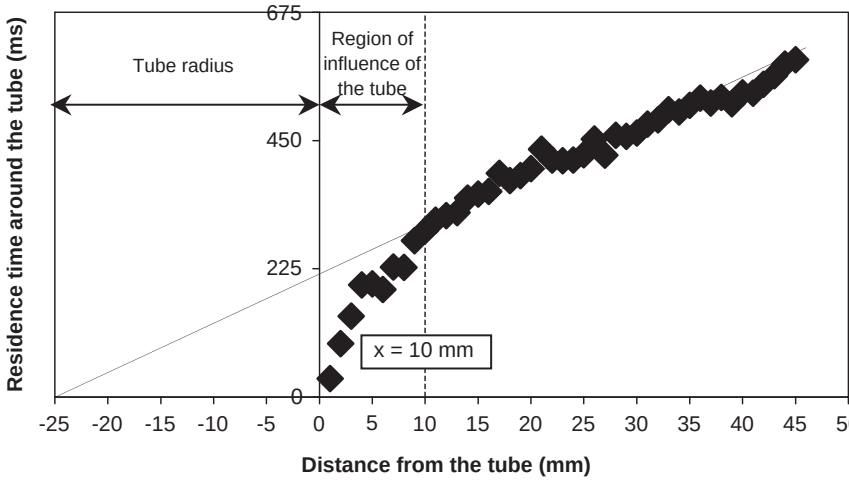

Figure 6 Variation in residence time around tube with increasing distance from the tube: rectangular bed (0.6 m × 0.06 m × 1.5 m), 0.6 mm sand, bed static height 400 mm and tube positioned at a bed level of 280 mm above the distributor (Wong and Seville, 2006).

Figure 6 shows the residence time around a tube, as a function of distance from the tube. Particles were taken randomly from the bulk to be irradiated as tracers. The tracking time for each experiment was approximately 1.5 h.

With increase in the thickness of the annulus inside which the residence time is obtained, it can be seen that there is a change in the slope of the residence time plot. As the thickness of the annulus becomes large by comparison with the radius of the tube, the presence of the tube becomes less significant and a linear relationship would be expected between residence time and annulus dimension (distance from the tube), as observed here for larger distances. The slope of the plot after 10 mm can be extended back to the tube centreline. The point at which the measurements deviate from this linear plot defines the ''region of influence'' of the tube. The thickness of the region of influence of the tube was estimated at approximately 10 mm, independent of gas velocity. Wong (2003) shows that the mean residence time within this region is inversely proportional to the square root of the excess gas velocity ($U–U_{mf}$), as suggested by Bock (1983).

3.1.3 Circulating fluidised beds

Circulating fluidised beds (CFBs) are attracting increasing interest for both gas–solid and gas-catalytic reactions; however, the operating modes in these two cases are completely different. In modelling and designing

CFBs as reactors, the solids residence time is an important parameter. Previous studies mostly assess operations at moderate values of the solids circulation rates ($\leq 100\,kg/m^2\,s$), whereas gas-catalytic reactions and, e.g., biomass pyrolysis require completely different operating conditions.

Van de Velden et al. (2008) used PEPT to study the movement and population density of particles in the CFB-riser. The PEPT results were used to obtain (i) the vertical particle movement and population density in a cross-sectional area of the riser; (ii) the transport gas velocity required to operate in a fully established circulation mode; (iii) the overall particle movement mode (core flow *versus* core/annulus flow); and (iv) the particle slip velocity. Figure 7 shows an example of PEPT data for the two principal flow regimes.

Using these results Van de Velden et al. (2008) were able to recommend design rules for operation of such reactors in terms of the gas velocity/solids loading parameters. For example, to ensure a narrow residence time distribution (operating, in effect, in plug flow), the superficial gas velocity should exceed the transport velocity by approximately 1 m/s and the solids circulation rate should exceed $200\,kg/m^2\,s$.

3.1.4 Validation of computational models

Hoomans et al. (2001) and Link et al. (2008) have used PEPT to validate computational approaches to the modelling of fluidised beds. In both cases, the computational method used was a 3D Euler–Lagrangian hard-sphere discrete particle model (DPM). Hoomans et al. (2001) simulated a conventional bubbling bed with a uniform gas distributor. Link et al. (2008) simulated the behaviour of a spout-fluid bed. In the hard-sphere collision model used in these studies, rigid particles are assumed to interact through binary, instantaneous collisions. Particle collision dynamics are described by collision laws, which account for energy dissipation due to non-ideal particle–particle and particle–wall interaction by means of the empirical coefficients of normal and tangential restitution, and the coefficient of friction. For systems that are not too dense, the hard-sphere model is considerably faster than soft-sphere models, which is why it was adopted for this work. The particle collision parameters play an important role in the overall bed behaviour, as reported by Goldschmidt et al. (2001), and were determined using impact experiments.

Results are reported by Link et al. (2008) of a combined experimental and simulation study on the flow regimes which can be encountered during operation of a spout-fluid bed. A regime map was composed, employing spectral analysis of pressure drop fluctuations and fast video recordings, and compared with the results of 3D computations. For most investigated regimes, the model is able to predict the appropriate regime.

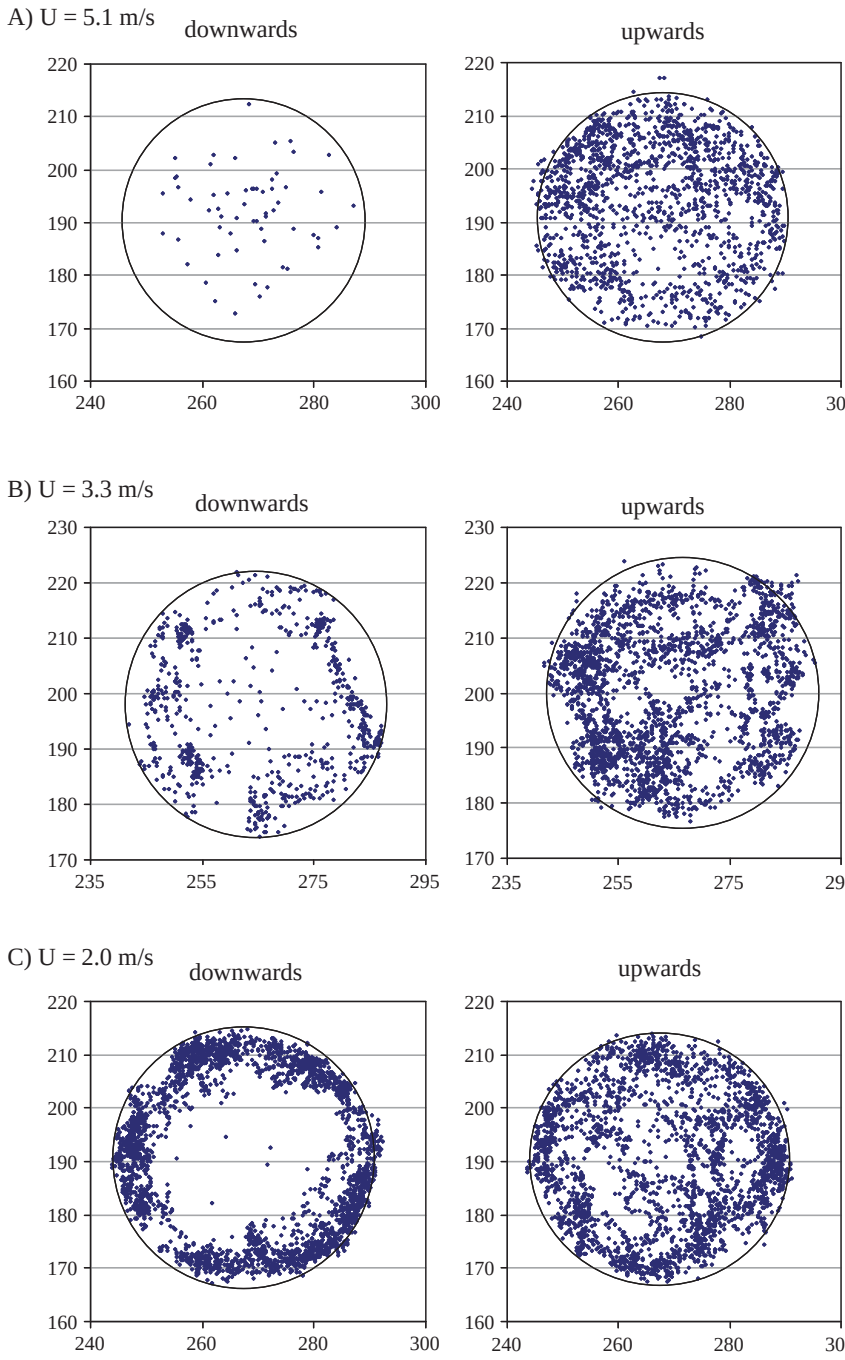

Figure 7 Cross-sectional view of the riser with left: downwards moving particles, and right: upwards moving particles; at $G = 260\,\mathrm{kg/m^2s}$ and indicated superficial gas velocity (U). The plots show all the particle locations over the height of the viewed section, integrated over the time of the run (Van de Velden et al., 2008).

The model is also able to reproduce the measured particle velocity profiles in the bed, including their distribution, for all investigated conditions.

3.2 Rotating drums and kilns

Industrial-scale rotating drums are usually operated in the rolling or slumping mode, according to whether the flow down the inclined surface is continuous or discontinuous, that is, in a series of avalanches. In either case, the bed can be divided into two regions (Figure 8): the ''passive'' region, in which the particles are carried up as a rigid body by the drum wall, and the ''active'' region in which they move down. Ding et al. (2001a, 2002) have shown that solids mixing and segregation occur largely in the active region, and will strongly influence bed-freeboard heat and mass transfer and therefore chemical reactions.

Solids exchange between the passive and active regions is important and an expression for the exchange coefficient between the regions has been developed, which is equivalent to a bed ''turnover'' frequency. An explicit relationship between turnover time and the drum operating parameters has been obtained and tested (Ding et al., 2002). The derivation of this relationship has led to an expression for the transition between the bed slumping and rolling conditions.

In continuous operation, the residence time distribution in a rotating drum depends on the degree of both radial and axial dispersion. In previous work (des Boscs et al., 1997), it was proposed that a particle in a distribution will have a preferred radial position, about which its actual position will be distributed, and will then experience an axial

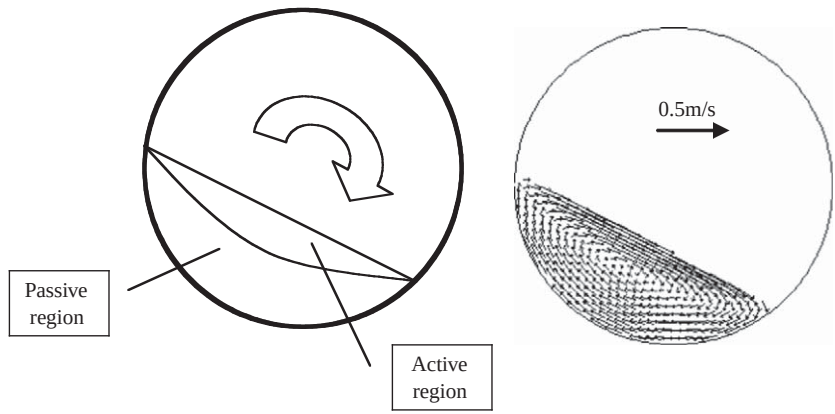

Figure 8 Particle motion in the transverse direction of a rotating drum: (a) schematic and (b) average velocity vectors from PEPT.

advancement per cycle which is statistically distributed around a most probable value corresponding to the angle of maximum slope. The distributions of particle position in successive cycles have been investigated, the most striking result being that even in the rolling mode, and with a narrow size distribution so that segregation is not expected, there is a strong correlation between the radii in the passive region before and after passage through the active layer (Ingram et al., 2005), that is, dispersion between layers is limited. This effect is more marked with wider size distributions, which rapidly segregate into distinct radial bands (Figure 9).

The charge in a rotating drum is also very prone to segregation in an axial direction. PEPT allows tracers of different sizes to be followed (Parker et al., 2005), so that the concentration of fines in the centre and coarse at the wall can be observed. In some cases (perhaps all), axial segregation occurs when the central core of fines running the entire length of the drum breaks out to the surface at regular intervals. PET has been used to image this effect (Figure 10), the first time this has been demonstrated.

3.3 Solids mixing

Both PEPT and PET have been used extensively in studies of solids mixing, in devices ranging from rotating vessels, such as kilns and V-mixers, to bladed mixers with both horizontal and vertical axes.

The V-mixer is a simple device, widely used in the pharmaceutical industry, which consists of two cylinders, joined at 90°, as shown in Figure 11 (Kuo et al., 2002, 2005). It rotates around the axis shown, thus, repeatedly dividing ($\wedge$) and recombining ($\vee$) the charge. At each rotation a small amount of material is transferred across the plane of symmetry between the two arms. The reason for studying this device is not because it is of great inherent interest in itself but because it is

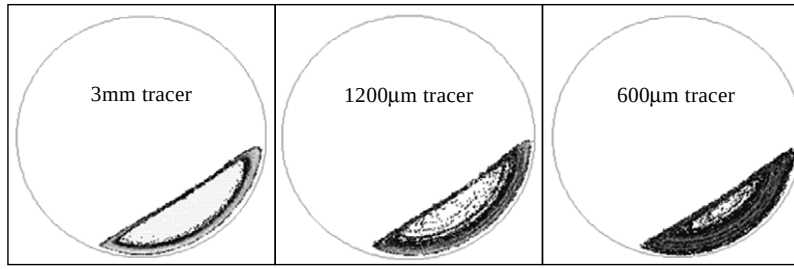

Figure 9 Transaxial PEPT occupancy plots (fraction of run time spent at each location) for three different sizes of tracer particle in a bed containing a wide range of particle sizes; dark indicates high occupancy.

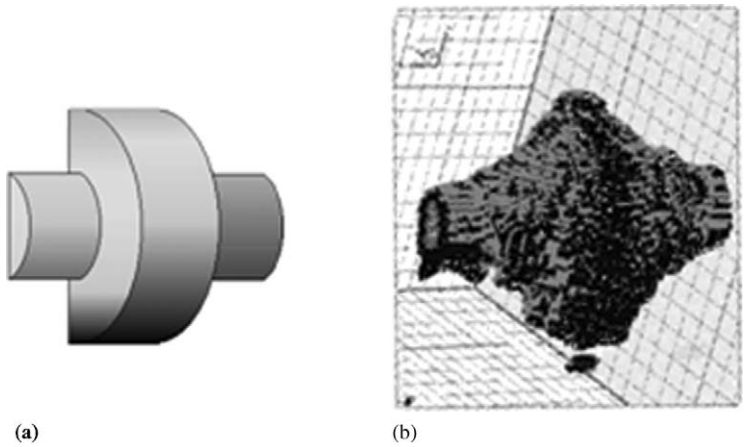

Figure 10 Axial banding of a binary mixture in a continuous-flow rotating drum: (a) schematic drawing showing the form of axial banding merging with a continuous core and (b) 3D PET image, showing the same features.

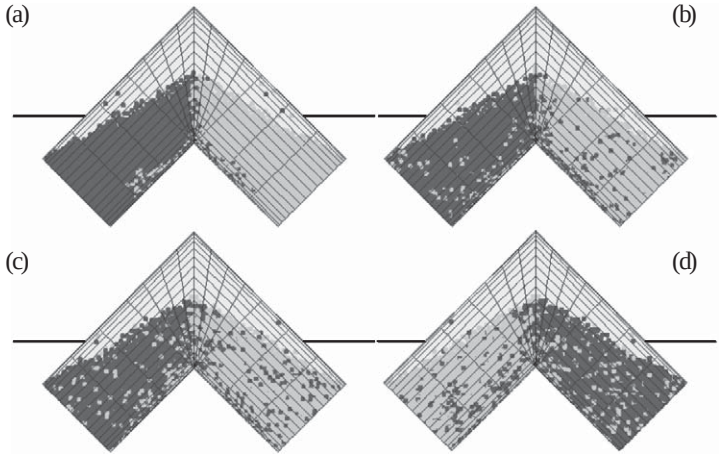

Figure 11 DEM simulations for 1 (a), 4 (b), 8 (c) revolutions in the front views and 8 revolutions in the back view (d) (Kuo et al., 2002).

representative of that generic class of mixers in which the solids are repeatedly divided and recombined. Typical results of discrete element modelling (DEM) studies of this device are shown in Figure 11.

One of the chief challenges in modelling is experimental validation, and single particle trajectory following using PEPT has proved useful in this. Figure 12 shows the close agreement that can be achieved between the average velocity distributions from both model and experiment. A

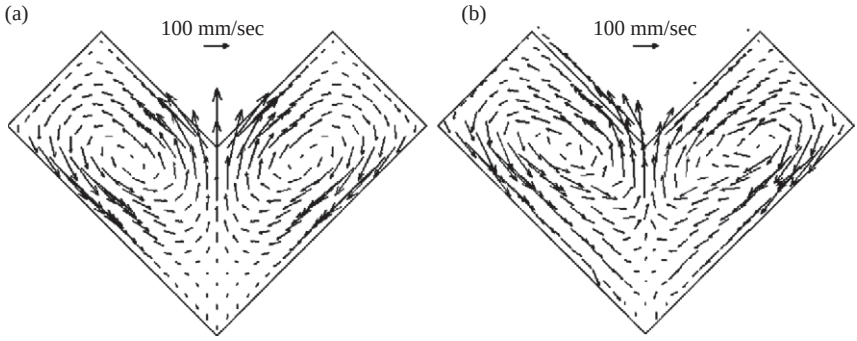

Figure 12 Velocity distributions at 20% fill, 60 rpm: (a) DEM simulations and (b) PEPT experiment (Kuo et al., 2002).

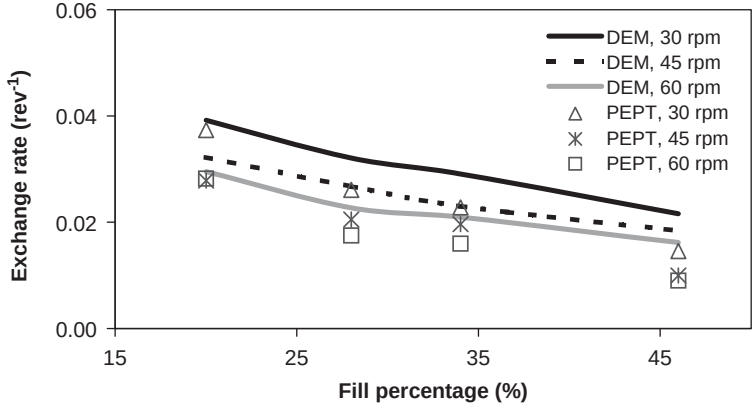

Figure 13 The exchange rate as a function of the fill percentage at different rotational speeds (Kuo et al., 2002).

more quantitative comparison between the two is provided by the exchange rate of solids across the dividing plane, which is plotted as a function of fill level in Figure 13 (the exchange rate is here defined as the probability that a single particle will swop sides per revolution). Again, the agreement is good. It is well-known that the exchange rate reduces as the fill level is increased, but this work also revealed the unexpected result that particle exchange during the division step is more important than during the combination step.

In all types of mixers it is useful to be able to quantify dispersion or particle mobility. Parker et al. (1997) showed that the axial dispersion coefficient, D, could be measured in rotating drums, for example, by plotting the mean value of (axial displacement, x_d)^2 versus time:

$$D = <x_{\mathrm{d}}^2>/2t \tag{2}$$

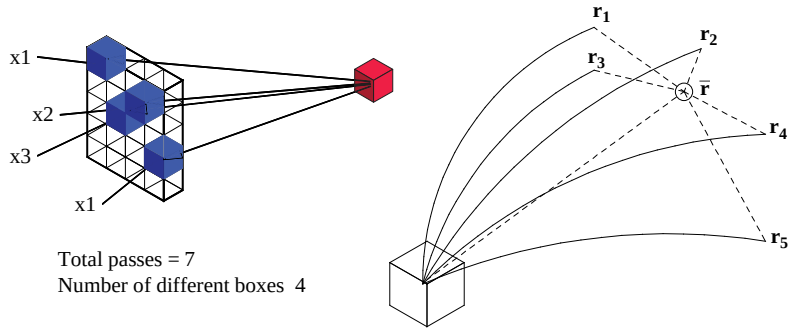

Figure 14 Analysis of dispersion (Martin et al., 2007).

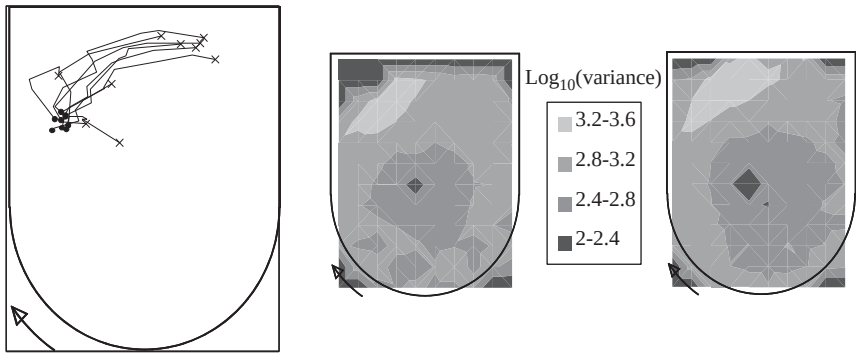

Figure 15 Analysis of dispersion in a high-speed bladed mixer (from Left to Right: multiple trajectories starting from the same volume element; two examples of distributions of variance (Martin et al., 2007).

More interesting, however, is to follow the dispersion of a group of particles originating at the same point (Martin et al., 2007) (Figure 14). The difference between the trajectories is a measure of dispersion related to processes occurring at that point. In single particle tracer studies, each time the tracer passes through a given volume element of the system, its subsequent location (some time or distance later) can be found. When the tracer has passed through each element many times, many traces are obtained with their origins at approximately the same point. Provided that the motion of the solids is time-independent, this is equivalent to tracing the path of many particles from the same location simultaneously. Figure 15 shows an example for a mixer with a high-speed rotating blade.

The variance between the locations is then given by

$$\sigma^2 = \frac{1}{n}\sum_{i=1}^{n}(x_i - \bar{x})^2 + (y_i - \bar{y})^2 + (z_i - \bar{z})^2 \qquad (3)$$

where σ is the standard deviation; $\bar{x}$, $\bar{y}$, $\bar{z}$ are the mean final location; and n is the number of traces.

The question arises as to how far (or for how long) the tracer particle should be allowed to move before its location variance is found. In the first place, time is a more appropriate measure for the interval between the start point and the variance measurement, and is consistent with the approach taken in diffusion. Secondly, the elapsed time should be enough to allow measurable movement to take place, but not so much that that movement is no longer related to the conditions which are local to the point of interest. In this particular example, the mixer used was of diameter 150 mm, and the maximum blade tip speed approximately 0.8 m/s. A ''dispersion time'' of 100 ms thus gives a maximum displacement of approximately 80 mm, which is about the same magnitude as the radius and consistent with the lengths of trajectories shown in Figure 15. An example of the distribution of the resulting variance is also shown in Figure 15.

To obtain a measure of the overall mixer effectiveness, account needs to be taken of the number of times each volume element is visited by the tracer; dividing by the total number of passes through all elements normalises these values. A measure of ''mixer effectiveness'' (ME) is then given by

$$\mathrm{ME} = \frac{1}{N_p} \sum_{i=1}^{n} \sigma_i^2 n_{pi} \tag{4}$$

where σ_i^2 is the variance for element i, n_{pi} the number of passes through element i, n the number of elements in the system and N_p the total number of passes.

In the example considered above, the maximum value of ME was approximately 1,050 mm^2.

Martin et al. (2007) showed how the choice of the time-for-dispersion discussed above affects the ME values. ME cannot increase without limit, because it is bounded by the physical size of the mixer. As expected, the ME versus time relationship is of the form:

$$\mathrm{ME} = \mathrm{ME}_\infty (1 - \mathrm{e}^{-\lambda t}) \tag{5}$$

where ME_∞ is the steady-state ME value at infinite time and λ is a (first-order) rate constant, although this relationship is affected by the existence of parallel mixing processes going on at different scales, for example, local to a blade and on the scale of the whole vessel.

PET is also of use in following mixing processes, although the time necessary to provide a complete tomographic scan of a piece of process equipment is still long — many minutes — so that it is normally necessary in such experiments to stop the process intermittently in order for periodic scans to take place. Armstrong et al. (2005) demonstrate the

Figure 16 PET image (right) of dispersion of a pseudo drug substance within an excipient contained in a mixing vessel (left) (Armstrong et al., 2005).

use of PET in following the mixing of a pharmaceutical active ingredient in a much larger bulk of excipient material, mixed within a polygonal rotating bin of the type used in the pharmaceutical industry for both intermediate storage and mixing (Figure 16).

3.4 Other applications

The scope of applications of PEPT is given in Table 1, which lists recent projects and includes brief notes on the significance of each as far as use of positron emission techniques are concerned. It will be noted that most applications to date are in gas-phase-continuous systems. PEPT can also be used in liquid-phase-continuous systems, where the challenge is to produce a truly flow-following tracer which does not lose its activity due to leaching into the liquid. Progress in liquid mixing studies is summarised by Barigou (2004), whereas Bakalis et al. (2004, 2006) demonstrate flow-following in viscous liquids. Fishwick et al. (2005a, b) show how PEPT has been used in helping to understand flow in multi-phase reactors.

4. PORTABLE PEPT

PEPT has become an established technique for studying the motion of particles in granular and fluid systems. Until recently, this technique was confined to use with medically derived detectors, which places constraints on the geometry and scale of process equipment that can be viewed. Demand for greater flexibility in the use of the PEPT

Table 1 Applications of PEPT

Project	Investigators[a]	Major outcomes in relation to PEPT[b]
Experimental and computational (DEM) study of fluidisation of cohesive particles	J.P.K. Seville and C. Thornton	First tracking of sub 100 μm particles in gas fluidisation, including under pressure (20 bars). Comparison with DEM predictions
Feasibility of tracking multiple tracers	P.J. Fryer, D.J. Parker and J.P.K. Seville	Multiple tracking algorithm development and experimental demonstration in fluidisation and solid/liquid flows
Application of particulate flavours to foodstuffs	P.J. Fryer and J.P.K. Seville	Tracking of difficult-to-label foodstuffs in rotating food processing machinery
Mixing of dense suspensions and rheologically complex opaque fluids	M. Barigou and A.W. Nienow	Tracking in large liquid-filled vessels (increased scatter) and at high speed with rapidly changing direction. Multimode comparisons with electrical resistance tomography and with CFD.
Development of multi-scale models for powder compaction processing	C.Y. Wu	Tracking of particles in die filling operations
Particle motion in 3D vibro-fluidised granular "gases"	R.D. Wildman (University of Loughborough)	High velocity, high accuracy motion required to extract granular temperature
Product–process relationships in high-shear granulation	M. Ghadiri, R.A. Williams, S. Anthony and Y. Ding (Leeds)	Motion inside metal-walled vessels of complex shape. Scale-up studies

Table 1 *(Continued)*

Project	Investigators[a]	Major outcomes in relation to PEPT[b]
Particle separation by vibrated liquid fluidised beds	M. Biggs, D. Glass and J.Y. Ooi (University of Edinburgh)	Vibrationary solids motion on a small scale in a liquid fluidised bed.
Powder processing in the pharmaceutical industry	J.P.K. Seville, D.J. Parker and A. Ingram	Both PEPT and PET used to characterise dispersion of drug mimic in mixing
Solids motion in circulating fluidised beds	J. Baeyens and J.P.K. Seville	First tracking measurements in circulating beds and cyclones
Coating in a pharmaceutical Wurster coater	J.P.K. Seville and A. Ingram	Provides fundamental input data to coating models
Solids motion in polymer extrusion	A. Ingram and J.P.K. Seville	Tracking molten polymer in thick-walled extruder+comparison with computational model from TU Eindhoven
Novel continuous granulation process	J.P.K. Seville and A. Ingram	Three-phase study in thick metal-walled vessel
Solids motion of polyethylene in fluidised bed reactor	J.P.K. Seville and A. Ingram	Comparison with CFD study by University of Toulouse
Solids motion in partitioned pilot scale fluidised bed	D.J. Parker, J.P.K. Seville and A. Ingram	First *in situ* study using mobile camera. Large-scale fluidisation
Solids motion in rotating waste pyrolyser	A. Ingram	Tracking large eccentric items
Bioseparation in expanded bed absorption columns	O.R.T. Thomas	Tracking 100 μm particles in fluidised chromatography columns

Table 1 *(Continued)*

Project	Investigators[a]	Major outcomes in relation to PEPT[b]
Minerals comminution	I. Govender (University of Cape Town)	Tracking mineral fragments and slurry in ball mills
Metals casting	W.D. Griffiths	First application of PEPT in high temperature liquid flows (molten aluminium) and comparison with computational models

[a]University of Birmingham except where stated.
[b]See publication list.

technique — in imaging larger process equipment and, more importantly, industrial equipment *in situ* — has led to the development of a modular PEPT camera (Leadbeater and Parker, 2009; Parker et al., 2008, 2009). This comprises a set of individual detectors, which can be arranged around the equipment in whatever configuration is appropriate to enable particle tracking. In an initial trial, the modular camera has been used to track particle motion in a 750 mm diameter pressurised fluidised bed reactor under industrially relevant conditions. The results show how the technique can be used reliably on large-scale equipment to measure quantities such as circulation time.

As discussed in Section 2, the present Birmingham positron camera, which has been used in almost all reported PEPT studies, consists of a single pair of large area detectors. In contrast, most medical PET scanners consist of rings of hundreds of small detectors. By distributing the events over many detection elements the problems of dead time and random coincidences are reduced so that higher overall count rates can be achieved. Since count rate is critical for tracking at high speed, it is of considerable interest to investigate extending this approach to PEPT. An important additional benefit of constructing a positron camera from a number of detector modules is that it becomes possible to consider adapting the detection geometry to suit the individual system under study.

A redundant medical PET scanner, a CTI ECAT931/08, was acquired. This comprises 128 detector blocks (Figure 2a), each consisting of four photomultiplier tubes viewing a 30 mm thick crystal of bismuth germanate scintillator approximately $49 \times 56\,\text{mm}^2$ in area, which is cut into an array of 8×4 elements (each approximately $5.6 \times 12.9\,\text{mm}^2$,

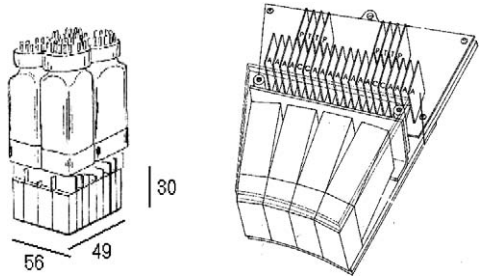

Figure 17 Components of the ECAT931 scanner: (left) detector block (dimensions in mm) and (right) 4 blocks mounted on a bucket (Parker et al., 2008a).

separated by slots 0.6 mm wide). By comparing the light intensities measured in the four photomultipliers, a γ-ray interaction can be unambiguously assigned to a particular element out of 32.

The blocks are grouped in sets of four into ''buckets'' (Figure 17) on which are mounted the appropriate electronics (preamplifiers and discriminators under microprocessor control). The buckets can thus be considered as detector modules (each with an active area of $200 \times 56\,\text{mm}^2$), and the scanner consists of 32 of these buckets. As originally configured they were mounted in two adjacent rings (16 buckets in each ring), so that in terms of the individual detection elements this corresponded to 8 rings each containing 512 elements.

The scanner is designed to recognise coincidences where events occur in two opposing buckets within a resolving time of 12 ns. In normal operation, only coincidences between two elements in the same ring or adjacent rings (of the 8) were accepted, but for PEPT use this restriction was removed. The data acquisition system of the scanner was also modified so that coincidence data is recorded in list mode with time stamps at 1 ms intervals.

The buckets were removed from the original gantry and reconfigured for trials as two rectangular arrays to mimic the geometry of the conventional positron camera. In considering the optimum layout of buckets, there is a trade-off between sensitivity and field of view. Because it is necessary to detect pairs of back-to-back γ-rays, tracking is only possible when the tracer lies directly between a pair of buckets. Taking into account the overlapping cones of detectable rays, the sensitivity is highest when the tracer lies on the centre line between the two buckets and drops to zero at the edge of the volume between (Figure 18). The same variation is found regardless of whether the buckets are directly opposite to each other or inclined at some angle, though the absolute sensitivity will depend on the orientation and separation. Maximum sensitivity will occur in regions which are in line between several pairs of buckets. On the other hand, to cover an extended field of view it is necessary to spread out the buckets.

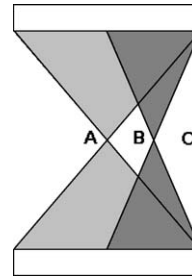

Figure 18 Schematic showing geometrical variation in sensitivity along the centre line between two detectors: at A, a wide cone of back-to-back gammas can be detected; at B, a narrower cone; and at C, the sensitivity drops to zero (Ingram et al., 2007).

Figure 19 (Left) Detector arrangement *in situ* next to lagged bed and (right) circulation arrangement, with central baffle; arrow shows additional gas injection (Ingram et al., 2007).

The first *in situ* industrial test was carried out at BP's Hull Research and Technology Centre in spring/summer of 2006 (Ingram et al., 2007) on a 750 mm diameter pilot scale fluidised bed with a central baffle plate and asymmetric gas injection to promote particle circulation, as shown in Figure 19. The fluid bed was operated under industrially relevant conditions of elevated temperature and pressure. Owing to the thickness of the lagging, the minimum detector separation was 1150 mm.

In this application, the portable camera is capable of imaging motion over the full width of the fluidised bed but not the full height. Because the main aim of the work was to quantify circulation, it was decided to form the camera elements up into lower and upper banks, intended to follow the flows under and over the baffle, respectively.

Figure 20 shows the tracer particle coordinates over a few seconds for this bed. The y coordinate in this case indicates height and the three shaded strips indicate the upper, middle and lower parts of the bed that are in the field of view. The x coordinate indicates which semi-cylindrical half of the bed the tracer is in. In general, particles were found to move up and down on each side of the central baffle, with occasional movement between semi-cylindrical sections, either under the baffle within the dense bed or over the baffle within the freeboard space. This trial demonstrated (a) the potential for PEPT to be used *in situ* in an industrial environment and (b) the practicality of the configurable layout.

5. SUMMARY AND FUTURE PLANS

In summary, among the most significant achievements of positron emission techniques in recent years are

- provision of realistic tracer particles for a wide range of applications,
- algorithm development and experimental demonstration of multi-particle PEPT,
- repeated demonstrations of the utility of the PEPT technique in validation of computational codes (CFD, DEM, etc.),
- parallel (and recently simultaneous) use of PEPT and electrical impedance tomography,
- parallel use of PEPT & PET in a dispersion/mixing problem,
- application of PEPT in novel fields: mineral engineering, metal casting, bioseparation, etc.,
- *in situ* large scale use of mobile PEPT on an industrial site.

PEPT and PET have great strengths but also certain limitations. Other measurement techniques (x-rays, magnetic resonance imaging, electrical impedance tomography, etc.) have complementary capabilities. Undoubtedly over the next few years there will be an increasing use of multi-modal studies, combining complementary measurement techniques either successively or simultaneously. For some applications, it will become important to be able to integrate PEPT data with computational simulations and data obtained from other modalities.

As in other imaging fields, developments in positron imaging occur in a symbiotic way: new capabilities enable new applications and new demands drive enhancement in capability. In capability development, there is a continuing demand to make tracers which are

- smaller — to extend the capability to its limits at the bottom end of the size range ($<50\,\mu$m),
- more active — to improve performance generally,

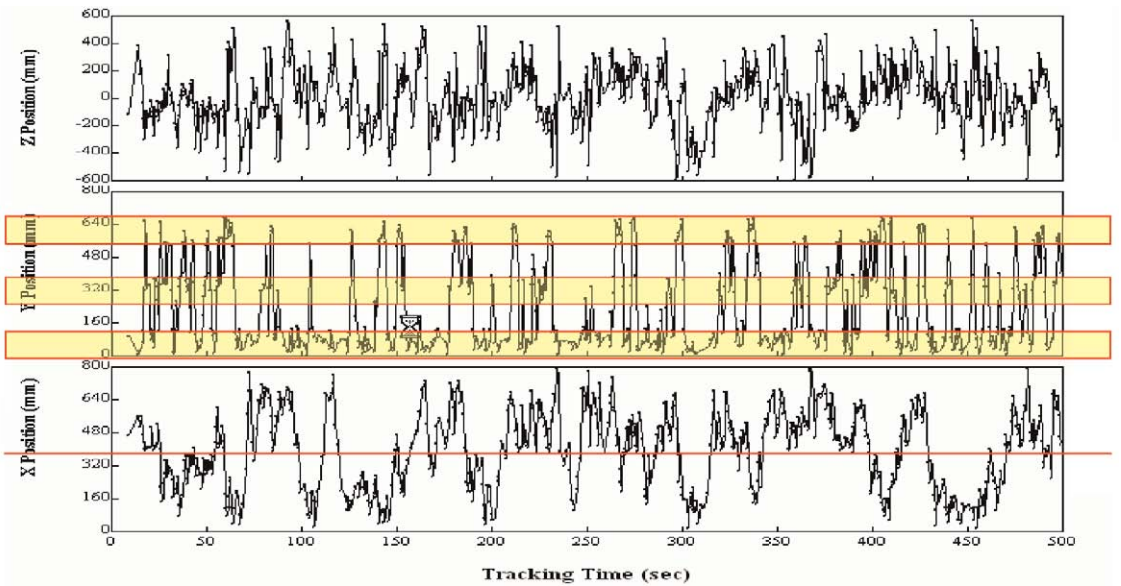

Figure 20 Tracer particle coordinates in 750 mm diameter bed. The *y* coordinate is vertical (Ingram et al., 2007).

- more robust — to withstand extremes of temperature, abrasion and chemical environment,
- more functional — with specific surface chemistry, so that they will follow one phase rather than another, for example.

Although PEPT is likely to remain the more appropriate choice for most industrially oriented positron-imaging work, PET can be useful in some circumstances, particularly for following slow processes such as diffusion and some classes of diffusion/reaction problems, as well as multi-phase pipeline flow.

In applications, increased capability in PEPT will enable more work with liquids and with multi-phase systems, and product-oriented studies aimed at probing the formation of microstructure. At the other extreme lies large-scale pilot- or process-level study which must be carried out *in situ*, using the new mobile PEPT camera. In large-scale applications, it will not in general be possible to provide trajectory information for the entire process volume. The challenge here is to develop ''minimal'' PEPT, in which location information is provided at as coarse a level as possible, consistent with the objectives of the study.

As mentioned earlier, work on validation of computational approaches to simulating multi-phase systems under realistic momentum and heat-transfer conditions is growing; PEPT represents one of very few ways of doing this convincingly.

SYMBOLS AND ABBREVIATIONS

D	axial dispersion coefficient
f	fraction of detected events actually used for PEPT location
ME	mixer effectiveness (Equation (4))
ME_∞	steady-state ME value at infinite time (Equation (5))
n	number of trajectory traces passing through a voxel
N	number of events detected during the location interval
N_p	total number of passes through all system voxels
t	time
w	intrinsic spatial resolution of the positron camera
x, y, z	location coordinates
$\bar{x}, \bar{y}, \bar{z}$	mean final location
x_d	axial displacement precision of a PEPT location (Equation (1))
λ	mixing rate constant
σ	standard deviation
PET	positron emission tomography
PEPT	positron emission particle tracking

ACKNOWLEDGEMENTS

This chapter expands on an earlier publication by Seville et al. (2005). The authors gratefully acknowledge the work of a number of colleagues and industrial collaborators, particularly Yulong Ding, Marc Hausard, Peter Knight, Hsui-Po Kuo, Tom Leadbeater, Tom Martin, David Newton, Vince Reiling, Matthias Stein and Charley Wu. Acknowledgement is also made to a succession of generous funding organisations, including the UK Engineering and Physical Sciences Research Council (EPSRC), the Biology and Biological Sciences Research Council (BBSRC), Unilever Research, BP, Innovene, GEA Pharma Systems and Yorkshire Forward.

REFERENCES

Armstrong, B., Fan, X., Ingram, A., and Parker, D. J., *in* "Particulate Systems Analysis 2005" RSC, London (2005).

Bakalis, S., Cox, P. W., Russell, A. B., Parker, D. J., and Fryer, P. J. *Chem. Eng. Sci.* **61**, 1864 (2006).

Bakalis, S., Fryer, P. J., and Parker, D. J. *AIChE J.* **50**, 1606 (2004).

Barigou, M. *Chem. Eng. Res. Des.* **82**, 1258 (2004).

Bock, H. J., 4th International Conference on Fluidization, paper 5.2.1, Kashikojima, Japan, preprints (1983).

Chaouki, J., Larachi, F., and Duduković, M. P., (Eds.), "Non-Invasive Monitoring of Multiphase Flows". Elsevier, Amsterdam (1997).

Depypere, F., Dewettinck, K., Pieters, J., Fan, X., Ingram, A., Parker, D. J., and Seville, J. P. K. (2009), unpublished work.

des Boscs, J. M., Seville, J. P. K., Parker, D. J., Ferlin, P., and Bourlier, C., Proceedings of IChemE Research Event, IChemE, Rugby, UK, p. 533 (1997).

Ding, Y. L., Forster, R. N. G., Seville, J. P. K., and Parker, D. J. *Chem. Eng. Sci.* **56**, 1769 (2001a).

Ding, Y. L., Forster, R. N. G., Seville, J. P. K., and Parker, D. J. *Powder Technol.* **124**, 18 (2002).

Ding, Y. L., Stein, M., Wong, Y. S., and Seville, J. P. K., *in* "Fluidization X" (M. Kwauk, J. Li, and W. C. Yang Eds.), p. 61. Engineering Foundation, New York (2001).

Fan, X., Parker, D. J., and Smith, M. D. *Nucl. Instrum. Methods* **A558**, 542 (2006a).

Fan, X., Parker, D. J., and Smith, M. D. *Nucl. Instrum. Methods A* **562**, 345 (2006b).

Fan, X., Parker, D. J., Smith, M. D., Ingram, A., Yang, Z. F., and Seville, J. P. K. *Nucl. Med. Biol.* **33**, 939 (2006c).

Fishwick, R., Winterbottom, J. M., Parker, D. J., Fan, X., and Stitt, H. *Can. J. Chem. Eng.* **83**, 97 (2005a).

Fishwick, R., Winterbottom, J. M., Parker, D. J., Fan, X., and Stitt, H. *Ind. Eng. Chem. Res.* **44**, 6371 (2005b).

Goldschmidt, M. J. V, Kuipers, J. A. M., and Swaaij, W. P. M. *Chem. Eng. Sci.* **56**, 571 (2001).

Hoomans, B. P. B., Kuipers, J. A. M., Mohd Salleh, M. A., Stein, M., and Seville, J. P. K. *Powder Technol.* **116**, 166 (2001).

Ingram, A., Hausard, M., Fan, X., Parker, D. J., Seville, J. P. K., Finn, N., Kilvington, R., and Evans, M, *in* "Fluidization XII" (F. Berruti, X. Bi, and T. Pugsley Eds.), p. 497. Engineering Conferences International, New York (2007).

Ingram, A., Seville, J. P. K., Parker, D. J., Fan, X., and Forster, R. N. G. *Powder Technol.* **158**, 76 (2005).

Kuo, H.-P., Burbidge, A. S., Knight, P. C., Parker, D. J., Tsuji, Y., and Seville, J. P. K. *Chem. Eng. Sci.* **57**, 3621 (2002).

Kuo, H. P., Knight, P. C., Parker, D. J., and Seville, J. P. K. *Powder Technol.* **152**, 133 (2005).

Leadbeater, T. W., and Parker, D. J., Nuclear Instruments and Methods in Physics Research Section A, in press (2009).
Leaper, M. C., Seville, J. P. K., Hilal, N., Kingman, S. W., and Burbidge, A. S. *Chem. Eng. Proc.* **43**(2), 187 (2004).
Link, J. M., Deen, N. G., Kuipers, J. A. M., Fan, X., Ingram, A., Parker, D. J., Wood, J., and Seville, J. P. K. *AIChE J.* **54**, 1189 (2008).
Martin, T. W., Seville, J. P. K., and Parker, D. J. *Chem. Eng. Sci.* **62**, 3419 (2007).
Mickley, H. S., and Fairbanks, D. F. *AIChE J.* **1**, 374 (1955).
Palmer, S. P., PhD Dissertation, University of Birmingham (2008).
Palmer, S. P., Ingram, A., Fan, X., Fitzpatrick, S., and Seville, J. P. K., *in* "Fluidization XII" (F. Berruti, X. Bi, and T. Pugsley Eds.), p. 433. Engineering Conferences International, New York (2007).
Parker, D. J., Dijkstra, A. E., Martin, T. W., and Seville, J. P. K. *Chem. Eng. Sci.* **52**, 2011 (1997).
Parker, D. J., Fan, X., Forster, R. N. G., Fowles, P., Ding, Y. L., and Seville, J. P. K. *Can. J. Chem. Eng.* **83**, 83 (2005).
Parker, D. J., Forster, R. N, Fowles, P., and Takhar, P. S. *Nucl. Instrum. Methods* **A477**, 540 (2002).
Parker, D. J., Leadbeater, T. W., Fan, X., Hausard, M. N., Ingram, A., and Yang, Z. *Meas. Sci. Technol.* **19**, 094004 (2008).
Parker, D. J., Leadbeater, T. W., Fan, X., Hausard, M. N., Ingram, A., Yang, Z., Nuclear Instruments and Methods in Physics Research Section A, in press (2009).
Seiler, C., Fryer, P. J., and Seville, J. P. K. *Can. J. Chem. Eng.* **86**, 571 (2008).
Seville, J. P. K., Ingram, A., and Parker, D. J. *Trans. Inst. Chem. Eng.* **83**, 788 (2005).
Seville, J. P. K, Salleh, A. M., Ingram, A., McCormack, A., Greenwood, R.W., and Reiling, V., *in* "Fluidization XI" (Arena, U., Chirone, R., Miccio, M., and Salatino, P. Eds.), p. 211. Engineering Conferences International, New York (2004).
Seville, J. P. K., Silomon-Pflug, H., and Knight, P. C. *Powder Technol.* **97**, 160 (1998).
Seville, J. P. K., Willett, C. D., and Knight, P. C. *Powder Technol.* **113**, 261 (2000).
Stein, M., Ding, Y. L, and Seville, J. P. K. *Chem. Eng. Sci.* **57**, 3649 (2002).
Stein, M., Ding, Y. L., Seville, J. P. K, and Parker, D. J. *Chem. Eng. Sci.* **55**, 5291 (2000).
Van de Velden, M., Baeyens, J., Seville, J. P. K, and Fan, X. *Powder Technol.* **183**, 290 (2008).
Wildman, R. D., Martin, T. W., Krouskop, P. E., Talbot, J., Huntley, J. M., and Parker, D. J. *Phys. Rev. E* **71**, 1539 (2005).
Wong Y. S., PhD Dissertation, University of Birmingham (2003).
Wong, Y. S., and Seville, J. P. K. *AIChE J.* **52**(12), 4099 (2006).
Yang, Z., Fan, X., Fryer, P. J., Parker, D. J., and Bakalis, S. *AIChE J.* **53**, 1941 (2007a).
Yang, Z., Fryer, P. J., Bakalis, S., Fan, X., Parker, D. J., and Seville, J. P. K. *Nucl. Instrum. Methods A* **577**, 585 (2007b).
Yang, Z., Parker, D. J., Fryer, P. J., Bakalis, S., and Fan, X. *Nucl. Instrum. Methods* **A564**, 332 (2006).